Single-photon emission of InAs/InP quantum dashes at 1.55 μm and temperatures up to 80 K

Ł. Dusanowski[1,a)], M. Syperek[1], J. Misiewicz[1], A. Somers[2], S. Höfling[2,3], M. Kamp[2], J. P. Reithmaier[2,4] and G. Sęk[1]

[1] *Laboratory for Optical Spectroscopy of Nanostructures, Division of Experimental Physics, Faculty of Fundamental Problems of Technology, Wrocław University of Science and Technology, Wybrzeże Wyspiańskiego 27, 50-370 Wrocław, Poland*

[2] *Technische Physik, University of Würzburg, Wilhelm-Conrad-Röntgen-Research Center for Complex Material Systems, Am Hubland, D-97074 Würzburg, Germany*

[3] *School of Physics and Astronomy, University of St. Andrews, North Haugh, KY16 9SS St. Andrews, United Kingdom*

[4] *Institute of Nanostructure Technologies and Analytics (INA), CINSaT, University of Kassel, Heinrich-Plett-Str. 40, 34132 Kassel, Germany*

Abstract

We report on single photon emission from a self-assembled InAs/InGaAlAs/InP quantum dash emitting at 1.55 μm at elevated temperatures. The photon auto-correlation histograms of the emission from a charged exciton indicate clear antibunching dips with as-measured $g^{(2)}(0)$ values significantly below 0.5 recorded at temperatures up to 80 K. It proves that charged exciton complex in a single quantum dash of the mature InP-based material system can act as a true single photon source up to at least liquid nitrogen temperature. This demonstrates the huge potential of InAs on InP nanostructures as non-classical light emitters for long-distance fiber-based secure communication technologies.

[a)] Corresponding author: lukasz.dusanowski@pwr.edu.pl

Single photons, due to their low decoherence, high speed transmission and many degrees of freedom are actually one of the most promising qubit implementations for the transmission of quantum information. Manipulation of single photons already allowed for the demonstration of free space quantum key distribution [1,2], simple quantum algorithms [3], CNOT-gates and entanglement manipulation following integrated photonic circuits approach [4,5]. Key elements of such systems are pure and efficient sources of single photons. It has been well established that exciton complexes confined within a self-assembled semiconductor quantum dot (QD) can be a true highly reliable microscopic single photon source (SPS) [6,7]. Due to the ability of monolithic integration of QDs with today's semiconductor devices it has become feasible to fabricate SPSs with extraordinary parameters, combining nearly perfect levels of photon purity and indistinguishability as well as high extraction efficiencies reaching at least 60-70 % [8,9]. Such state-of-the-art technology is currently based on the GaAs material system and so far, most progress has been made for nanostructures emitting photons with wavelengths shorter than 1 µm. Nevertheless, long distance quantum information technologies utilizing fiber-based optical communication technologies demand SPSs operating at the lowest loss telecommunication wavelengths at around 1.3 and 1.55 µm. Telecommunication wavelength emission can be achieved in GaAs system by combining InAs QDs with an additional InGaAs strain relaxation layer to increase the emission wavelength up to 1.3 [1,10–12] and even 1.55 µm [13]. Following this approach single photon emission has been demonstrated up to 1.3 µm [1,11], which allowed for successful quantum key distribution over 35 km using standard optical fibers at elevated temperatures [1].

An alternative technology, essential for the fabrication of structures at telecommunication wavelengths is based on the InAs/InP material system. QDs in such

material system have been already shown to be efficient and pure single photon emitters at wavelengths including both the second [14–16] and third [17–21] telecom band windows. High extraction efficiencies up to 46 % [16] and Purcell enhancement of the spontaneous emission rate as large as 5 [20] have been already reported by successfully embedding InAs/InP QDs into different kinds of optical resonator structures including photonic crystal [16,20] and micropillar [22] cavities or optical horn structures [17]. Only recently, 120 km range single photon quantum key distribution was demonstrated based on InAs/InP quantum dots with the second order correlation function at zero delay reaching values as low as 0.0051 [21]. Moreover, InAs/InP QDs embedded into photonic crystal cavities allowed for the first demonstration of on-demand 1.3 µm wavelength single photons with indistinguishabilities of 0.18 probed by two-photon interference measurements [16].

In this letter we investigate InAs/InGaAlAs/InP quantum dashes (QDashes), i.e. nanostructures which are strongly elongated in one of the in-plane directions, as potential telecom wavelength single photon emitters being able to operate at elevated temperatures. We report on single-photon emission at a temperature of 80 K from a charged exciton complex emitting at around 1.55 µm. The charged character of this complex is revealed by polarization-resolved photoluminescence measurements, in compliance with our previous studies [19]. Experiments have been performed on charged exciton emission since the lack of the fine structure splitting of the charged exciton results in higher single-photon emission repetition rates compared to the neutral exciton ones [23]. By performing systematic studies of photoluminescence and photon emission statistics spectroscopy as a function of temperature, we demonstrate that such kind of nanostructure can be considered as a promising telecommunication C-band single photon source operating at liquid nitrogen temperatures. Furthermore, it is an important step towards thermoelectrically cooled

telecom-band QDash-based SPSs, which should be achievable after further structure optimizations leading to increased quantum efficiencies and decreased thermal losses via the band structure and confinement engineering [24].

In ref.[25], the influence of changing the population of phonons (via increasing temperature) on the exciton decoherence was studied both theoretically and experimentally in case of strongly asymmetric InAs/InP nanostructures. It was shown that the structural geometry has a major influence on the exciton-acoustic-phonon coupling strength. For strongly elongated nanostructures such as QDashes, the influence of the phonon-related decoherence is expected to be significantly weaker in comparison to typical QDs, but it cannot be entirely neglected and dominates the emission spectra above 100 K. Moreover, theoretical studies performed for QDashes with lengths larger than 150 nm predict weak decoherence even above 200 K [26]. These results suggest that photons emitted from exciton complexes confined within InAs/InP QDashes should be much more robust against acoustic-phonons impact in comparison to more symmetric systems, which promises that QDashes might be well suited as telecom single photon sources operating at elevated temperatures. In this letter we make the first step in this direction and verify if indeed InAs/InP QDash nanostructures are able to generate single photons at elevated temperatures, reaching at least the practical limit of cooling by liquid nitrogen cooling (~77 K).

The investigated sample was grown in an EIKO gas source molecular-beam epitaxy system on a S-doped InP(001) substrate. The layer sequence starts from a 200 nm-thick $In_{0.53}Ga_{0.23}Al_{0.24}As$ layer lattice matched to InP, which was grown on the substrate at 500 °C. In order to form QDashes in a self-assembled way, an InAs layer with a nominal thickness of 1.3 nm was deposited at 470 °C, out of which QDash structures on a wetting layer were formed. The QDashes were covered by a 100 nm-thick $In_{0.53}Ga_{0.23}Al_{0.24}As$ layer and

subsequently capped with a 10 nm-thick layer of InP. Due to the atom's surface diffusion coefficient anisotropy, the epitaxially formed nanostructures are significantly elongated in one of the in-plane directions (preferentially [1-10]) [27]. The typical lateral dimensions of QDashes under this study are about 20 nm in width and between 50 and hundreds of nanometers in length, whereas their height is approximately 3.5 nm [28]. Since the planar density of QDashes is rather high – 5 x 10^{10} cm^{-2}, a combination of electron beam lithography and etching techniques has been used to produce mesa structures with different sizes down to 0.125 μm^2 (500x250 nm^2) in order to resolve the emission from single QDashes in an inhomogeneous ensemble.

For all the experiments, the sample was kept in a liquid-helium continuous-flow cryostat equipped with a heating wire attached to a PID temperature regulator loop for sample temperature control. Spatially-resolved photoluminescence spectroscopy and photon autocorrelation statistic measurements have been performed using a micro-photoluminescence (μPL) setup providing a spatial resolution on the order of a single μm, and a spectral resolution of approx. 100 μeV. The sample was excited with a 787 nm line of a continuous-wave (cw) semiconductor diode laser. The emission intensity of the isolated spectral lines has been detected by a liquid nitrogen-cooled InGaAs-based linear array detector combined with a 0.3 m focal length single grating monochromator. The degree of linear polarization has been measured by rotating a half-wave plate inserted in front of a linear polarizer placed at the monochromator entrance slit. Photon auto-correlation experiments were conducted with a Hanbury Brown and Twiss setup (HBT). In this case, two short focal length monochromators with approx. 0.1 nm spectral resolution were used as spectral filters for the selected wavelengths corresponding to the charged exciton emission. Each of the monochromator outputs was equipped with a fiber-coupled NbN

superconducting single-photon detector with ~15 % quantum efficiency and ~10 dark counts/s at 1.55 µm. The photon correlation statistics was acquired by a multichannel picosecond event timer. The overall temporal resolution of the system was ~80 ps.

Figure 1(a) shows the low temperature (T = 5 K) µPL spectra revealing a dominant emission line named CX from a QDash enclosed within a mesa structure of 500 x 250 nm^2 size. The spectrum was recorded under an excitation power of ~4 µW (measured outside the cryostat). The CX line is centered at 0.8072 eV. The intensity of this CX line as a function of excitation power exhibits a close to linear dependence before saturating at an excitation power of ~10 µW (inset in Fig. 1). This suggests neutral or charged exciton complex emission. Fig. 1(b) presents the spectral evolution of the CX line as a function of the linear polarization angle. The CX line energy reveals no polarization dependence within our setup resolution, indicating charged character of CX line [19]. In contrary to our previous results [19,29], we were not able to find any other exciton complexes originating from the same QDash. The nearest two neighboring emission lines visible above the CX energy at a distance of 2.8 and 4.3 meV (Fig. 2) are attributed to the emission of excitons from other individual QDashes, since cross-correlation measurements did not reveled any mutual time dependencies. CX line emission is significantly polarized with the degree of linear polarization (DOLP) of ~60 % along the elongation axis. Such a high value of DOLP can be attributed to the combination of valence-band mixing effect being an intrinsic property of QDashes [30,31], and rectangular shape of a mesa structure, geometry of which causes an enhancement of coupling between the quantum emitter and the optical field mode of a certain polarization [32].

In Figure 2 the temperature dependence of the µPL spectrum of a single InAs/InP QDash from a 500 x 250 nm^2 mesa is presented. For clarity, each spectrum has been normalized to the maximum of intensity. The line identified as a charged exciton CX can be

easily followed in the entire temperature range. The graph shows a considerable and natural redshift of the luminescence peaks due to the band gap shrinkage (Fig.3(b)) with increasing temperature. At a temperature of 80 K, the CX line energy is shifted by ~6.2 meV with respect to low temperature spectra, allowing for the generation of ~1548 nm photons. At low temperatures of 5-30 K the CX peak exhibits a Gaussian profile with linewidth of ~0.2 meV, indicating the inhomogeneous impact of the environment on the QDash emission [33]. With increasing temperature sidebands appear, due to the coupling of the CX complex to acoustic phonons [25]. The temperature dependence of the CX emission line full width at half-maximum (FWHM) is presented in Fig. 3(a). The spectral linewidth increases with temperature, eventually broadening to ~0.67 meV at 80 K. It resembles a typical behavior predicted for quantum dash exciton with reduced phonon coupling strength due to the enlarged and anisotropic wave-function extension [25]. The inset in Fig. 2 presents the μPL signal of the CX line plotted versus inverse temperature. The intensity of the CX line drops fivefold when the temperature is increased from 5 up to 80 K. This data was fitted by the Arrhenius formula (solid line) whereby the thermal quenching activation energy equal to ~20 meV was obtained. Such a value of activation energy may be associated with electrons escaping from the QDashes directly to the wetting layer [24].

The second order photon auto-correlation functions $g^{(2)}(\tau)$ of this CX emission have been recorded under cw excitation for various temperatures. In Figures 4(a)-4(d) the auto-correlation histograms for the charged exciton line are displayed for temperatures of 5, 30, 55 and 80 K, correspondingly. The excitation power used for these measurements was kept around ~3-6 μW (depending on the temperature), well below the saturation power of the CX emission (~10 μW). The excitation power has been increased slightly with temperature, which allowed compensating the reduction of the photon count rate due to the thermal

quenching. All the recorded $g^{(2)}(\tau)$ functions show clear photon antibunching dips at zero time delay with $g^{(2)}(0)$ values significantly below the 0.5 limit. The low temperature histograms (up to 30 K) show $g^{(2)}(0)$ values around ~0.18-0.19. Non-zero $g^{(2)}(0)$ values are most likely due to the combination of the system background counts, large time bin (256 ps) and limited time resolution of the HBT setup (~80 ps). By performing the data fitting with a standard second order correlation function $g_R^{(2)}(\tau) = 1 - \left(1 - g_R^{(2)}(\tau = 0)\right)\exp\left(-\frac{|\tau|}{\tau_f}\right)$ convoluted with the system instrumental response function (IRF) in the form of $\exp\left(-\frac{|\tau|}{\tau_{IRF}}\right)$, where τ_{IRF} is setup time resolution (80 ps), the resulting $g_R^{(2)}(0)$ for both histograms reaches almost zero value (see the dashed line in Fig. 4). The antibunching time constant τ_f was determined to be 0.48 and 0.46 at temperatures of 5 and 30 K, respectively. Such small values of τ_f in respect to predicted radiative lifetimes (1-2 ns [29]) suggest that CX occupation changes and therefore also $g^{(2)}(\tau)$ build-ups are limited mainly by high photoexcitation rates [34]. With increasing temperature, $g^{(2)}(0)$ values increase from ~0.23 at 55 K to ~0.34 at 80 K (Figs. 4(c) and 4(d)). The observed decrease of the single photon emission purity may be attributed to the background photons emitted from the neighboring QDashes which become pronounced at higher temperatures due to the acoustic-phonon-related sidebands (80 K spectra in Fig. 2). To estimate the background influence on the $g^{(2)}(0)$ value, we performed a rough signal (S) to background (B) ratio estimation $\rho = S/(S+B)$, where S was taken as the CX peak intensity and B as a mean of low and high energy background intensity of the CX peak. Assuming a Poissonian background character, the measured $g^{(2)}(0)$ value should be increased by $1-\rho^2$ factor [35]. For 55 K (80 K) temperature ρ was determined to be 0.89 (0.84) resulting in a $g_B^{(2)}(0) = 1-\rho^2$ value of ~0.21 (~0.29). The obtained values of $g_B^{(2)}(0)$ are slightly overestimated taking into account additional effect of

IRF (for 55 K: 0.18 + 0.21 > 0.23), which may be a result of rather simplified background counts determination method. Despite this inconsistency, such rough estimation of the background points out at a non-negligible influence of neighboring QDashes on photon statistics at elevated temperatures. This effect may be suppressed in future by better separation of QDashes for example by modifying sample growth mode in order to reduce the nanostructures' surface densities.

In conclusion, we have investigated the temperature dependence of photon emission from single InAs/InGaAlAs/InP quantum dash emitting at 1.55 µm by µPL and photon-correlation spectroscopy. Single-photon emission has been verified under cw non-resonant optical excitation on charged exciton emission. Charged character of exciton complex has been confirmed by power-dependent and polarization resolved µPL. We were able to observe single photon emission up to temperature of 80 K with raw value of $g^{(2)}(0)$ equal to ~0.34, proving that the investigated structures can be considered as true single photon emitters able to operate at telecommunication wavelengths at liquid nitrogen temperatures. This is a promising result and an important milestone with respect to the practical application of InAs on InP epitaxial nanostructures in quantum information technologies.

Acknowledgements

This research was supported by the National Science Center of Poland within Grant No. 2011/02/A/ST3/00152.

References:

[1] P.M. Intallura, M.B. Ward, O.Z. Karimov, Z.L. Yuan, P. See, A.J. Shields, P. Atkinson, and D.A. Ritchie, Appl. Phys. Lett. **91**, 161103 (2007).

[2] M. Rau, T. Heindel, S. Unsleber, T. Braun, J. Fischer, S. Frick, S. Nauerth, C. Schneider, G. Vest, S. Reitzenstein, M. Kamp, A. Forchel, S. Höfling, and H. Weinfurter, New J. Phys. **16**, 043003 (2014).

[3] B.P. Lanyon, T.J. Weinhold, N.K. Langford, M. Barbieri, D.F. V James, A. Gilchrist, and A.G. White, Phys. Rev. Lett. **99**, 250505 (2007).

[4] H. Jin, F.M. Liu, P. Xu, J.L. Xia, M.L. Zhong, Y. Yuan, J.W. Zhou, Y.X. Gong, W. Wang, and S.N. Zhu, Phys. Rev. Lett. **113**, 103601 (2014).

[5] J. Wang, A. Santamato, P. Jiang, D. Bonneau, E. Engin, J.W. Silverstone, M. Lermer, J. Beetz, M. Kamp, S. Höfling, M.G. Tanner, C.M. Natarajan, R.H. Hadfield, S.N. Dorenbos, V. Zwiller, J.L. O'Brien, and M.G. Thompson, Opt. Commun. **327**, 49 (2014).

[6] S. Buckley, K. Rivoire, and J. Vučković, Rep. Prog. Phys. **75**, 126503 (2012).

[7] P. Michler, A. Kiraz, C. Becher, W. V Schoenfeld, P.M. Petroff, L. Zhang, E. Hu, and A. Imamoğlu, **290**, 2282 (2000).

[8] X. Ding, Y. He, Z.-C. Duan, N. Gregersen, M.-C. Chen, S. Unsleber, S. Maier, C. Schneider, M. Kamp, S. Höfling, C.-Y. Lu, and J.-W. Pan, Phys. Rev. Lett. **116**, 020401 (2016).

[9] N. Somaschi, V. Giesz, L. De Santis, J.C. Loredo, M.P. Almeida, and G. Hornecker, arXiv **1510.06499**, (2015).

[10] B. Alloing, C. Zinoni, V. Zwiller, L.H. Li, C. Monat, M. Gobet, G. Buchs, A. Fiore, E. Pelucchi, and E. Kapon, Appl. Phys. Lett. **86**, 101908 (2005).

[11] M.B. Ward, O.Z. Karimov, D.C. Unitt, Z.L. Yuan, P. See, D.G. Gevaux, A.J. Shields, P. Atkinson, and D.A. Ritchie, Appl. Phys. Lett. **86**, 201111 (2005).

[12] M. Strauss, S. Höfling, and A. Forchel, Nanotechnology **20**, 505601 (2009).

[13] E.S. Semenova, R. Hostein, G. Patriarche, O. Mauguin, L. Largeau, I. Robert-Philip, A. Beveratos, and A. Lemaître, J. Appl. Phys. **103**, 103533 (2008).

[14] K. Takemoto, Y. Sakuma, S. Hirose, T. Usuki, N. Yokoyama, T. Miyazawa, M. Takatsu, and Y. Arakawa, Jpn. J. Appl. Phys. **43**, L993 (2004).

[15] D. Elvira, R. Hostein, B. Fain, L. Monniello, A. Michon, G. Beaudoin, R. Braive, I. Robert-Philip, I. Abram, I. Sagnes, and A. Beveratos, Phys. Rev. B **84**, 195302 (2011).

[16] J. Kim, T. Cai, C.J.K. Richardson, R.P. Leavitt, and E. Waks, arXiv **1511.05617**, (2015).

[17] K. Takemoto, M. Takatsu, S. Hirose, N. Yokoyama, Y. Sakuma, T. Usuki, T. Miyazawa, and Y. Arakawa, J. Appl. Phys. **101**, 081720 (2007).

[18] M. Benyoucef, M. Yacob, J.P. Reithmaier, J. Kettler, and P. Michler, Appl. Phys. Lett. **103**, 162101 (2013).

[19] Ł. Dusanowski, M. Syperek, P. Mrowiński, W. Rudno-Rudziński, J. Misiewicz, A. Somers, S. Höfling, M. Kamp, J.P. Reithmaier, and G. Sęk, Appl. Phys. Lett. **105**, 021909 (2014).

[20] M.D. Birowosuto, H. Sumikura, S. Matsuo, H. Taniyama, P.J. van Veldhoven, R. Nötzel, and M. Notomi, Sci. Rep. **2**, 321 (2012).

[21] K. Takemoto, Y. Nambu, T. Miyazawa, Y. Sakuma, T. Yamamoto, S. Yorozu, and Y. Arakawa, Sci. Rep. **5**, 14383 (2015).

[22] S. Frederick, D. Dalacu, D. Poitras, G.C. Aers, P.J. Poole, J. Lefebvre, D. Chithrani, and R.L. Williams, Microelectronics J. **36**, 197 (2005).

[23] S. Strauf, N.G. Stoltz, M.T. Rakher, L.A. Coldren, P.M. Petroff, and D. Bouwmeester, Nat. Photonics **1**, 704 (2007).

[24] P. Podemski, R. Kudrawiec, J. Misiewicz, A. Somers, R. Schwertberger, J.P. Reithmaier, and A. Forchel, Appl. Phys. Lett. **89**, 151902 (2006).

[25] Ł. Dusanowski, A. Musiał, A. Maryński, P. Mrowiński, J. Andrzejewski, P. Machnikowski, J. Misiewicz, A. Somers, S. Höfling, J.P. Reithmaier, and G. Sęk, Phys. Rev. B **90**, 125424 (2014).

[26] Ł. Dusanowski, A. Musiał, G. Sęk, and P. Machnikowski, Acta Phys. Pol. A **124**, 813 (2013).

[27] J. Brault, M. Gendry, G. Grenet, G. Hollinger, Y. Desières, and T. Benyattou, Appl. Phys. Lett. **73**, 2932 (1998).

[28] A. Sauerwald, T. Kümmell, G. Bacher, A. Somers, R. Schwertberger, J.P. Reithmaier, and A. Forchel, Appl. Phys. Lett. **86**, 253112 (2005).

[29] Ł. Dusanowski, M. Syperek, W. Rudno-Rudziński, P. Mrowiński, G. Sęk, J. Misiewicz, A. Somers, J.P. Reithmaier, S. Höfling, and A. Forchel, Appl. Phys. Lett. **103**, 253113 (2013).

[30] P. Kaczmarkiewicz and P. Machnikowski, Semicond. Sci. Technol. **27**, 105012 (2012).

[31] A. Musiał, P. Kaczmarkiewicz, G. Sęk, P. Podemski, P. Machnikowski, J. Misiewicz, S. Hein, S. Höfling, and A. Forchel, Phys. Rev. B **85**, 035314 (2012).

[32] P. Mrowiński, K. Tarnowski, J. Olszewski, A. Somers, M. Kamp, S. Höfling, J.P. Reithmaier, W. Urbańczyk, J. Misiewicz, P. Machnikowski, and G. Sęk, Acta Phys. Pol. A **129**, A48 (2016).

[33] J. Seufert, R. Weigand, G. Bacher, T. Kümmell, A. Forchel, K. Leonardi, and D. Hommel, Appl. Phys. Lett. **76**, 1872 (2000).

[34] D. Regelman, U. Mizrahi, D. Gershoni, E. Ehrenfreund, W. Schoenfeld, and P. Petroff, Phys. Rev. Lett. **87**, 257401 (2001).

[35] K. Sebald, P. Michler, T. Passow, D. Hommel, G. Bacher, and A. Forchel, Appl. Phys. Lett. **81**, 2920 (2002).

Figure captions:

FIG. 1. (a) Low temperature (5 K) microphotoluminescence spectra from a charged exciton (CX) confined in a InAs/InP quantum dash excited cw at 787 nm. Inset: excitation power dependence of the CX peak intensity in log-log scale. (b) Polarization resolved microphotoluminescence spectral map for CX emission.

FIG. 2. (a) Temperature dependence of the PL spectra (normalized to maximum intensity) from single mesa structure with InAs/InP QDashes in the range of 5-80 K recorded at excitation power equal to 3 μW. Inset: inverse temperature dependence of intensity of the CX line photoluminescence. The solid line is a fit to the data yielding an activation energy of 20 meV.

FIG. 3. (a) Temperature dependence of CX line full width at half-maximum. (b) Temperature dependence of CX energy.

FIG. 4. Coincidence counts histograms recorded at temperatures 5 K (a), 30 K (b), 55 K (c) and 80 K (d) from CX emission. The solid line with shaded area presents the raw experimental data, the red dotted line presents fit of experimental data using second order correlation function $g^{(2)}(t)$ convoluted with the instrumental response function (IRF). Raw values of $g^{(2)}(0)$ are obtained without any data post-processing. A clear antibunching dip with $g^{(2)}(0) < 0.5$ is observed in all cases.

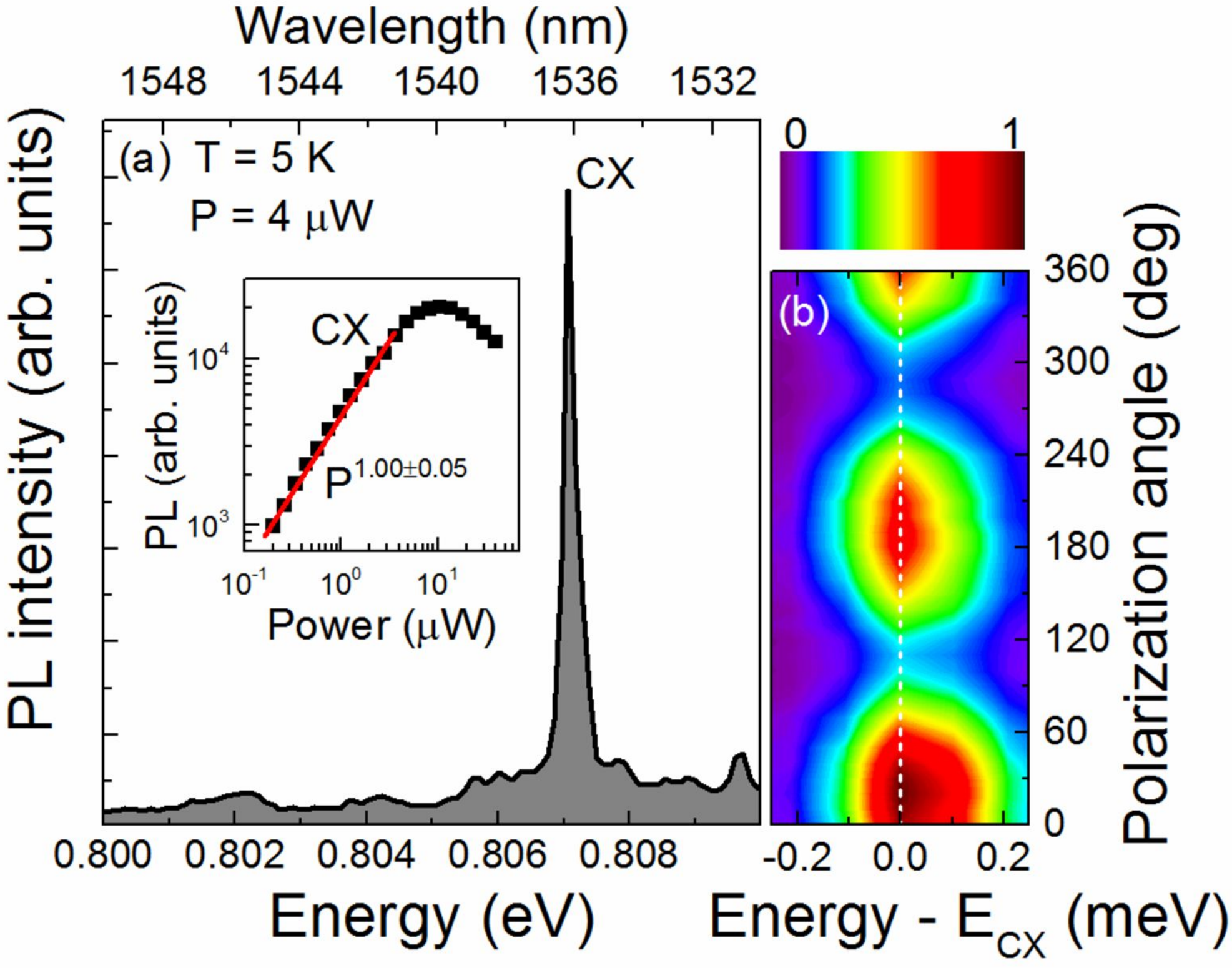
Wavelength (nm)
1548
1544
1540
1536
1532
(a) T = 5 K
P = 4 μW
CX
PL intensity (arb. units)
0.800
0.802
0.804
0.806
0.808
Energy (eV)
PL (arb. units)
10^4
10^3
CX
P^1.00±0.05
10^-1
10^0
10^1
Power (μW)
0
1
(b)
360
300
240
180
120
60
0
Polarization angle (deg)
-0.2
0.0
0.2
Energy - E_CX (meV)

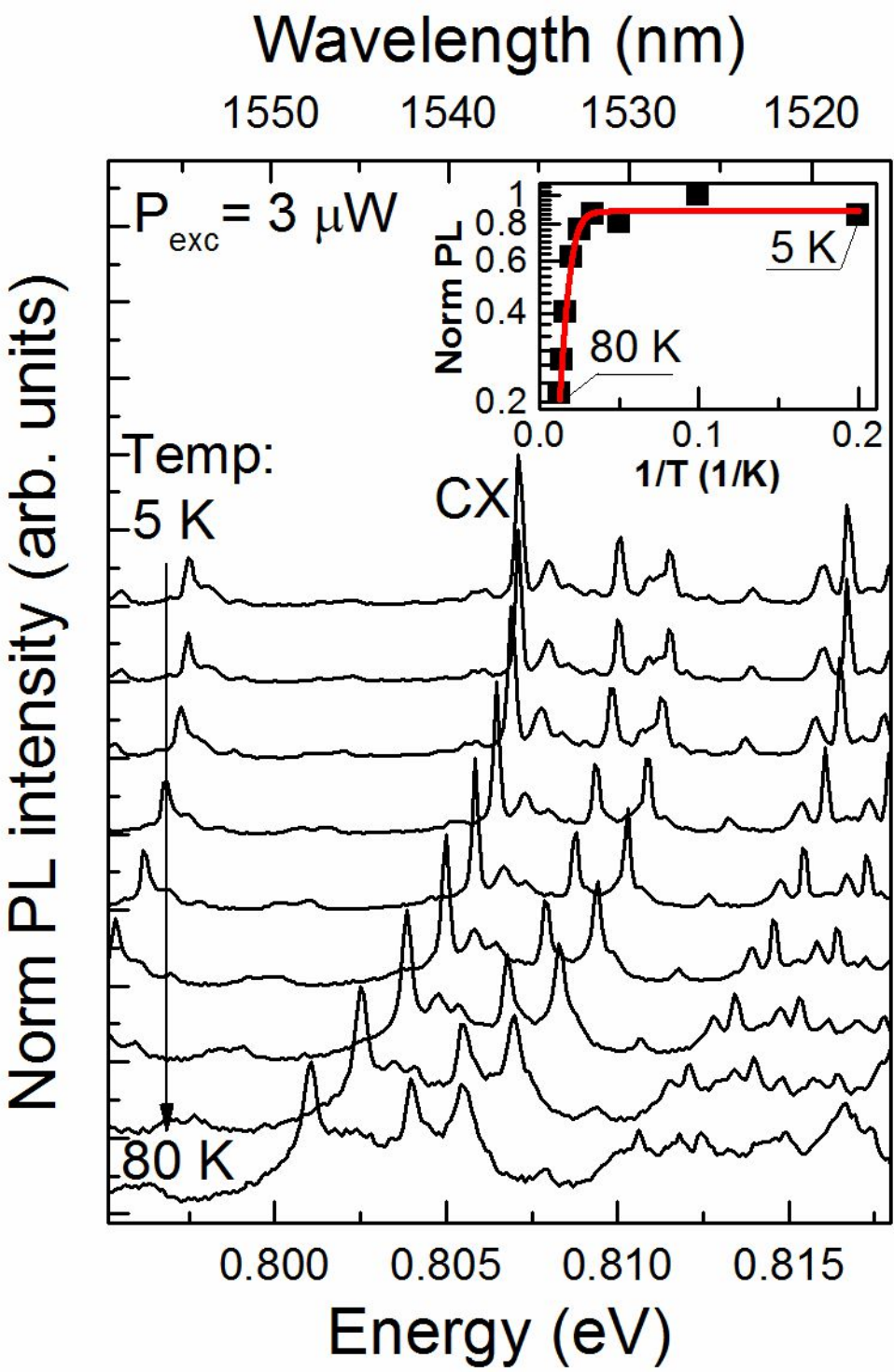
Wavelength (nm)
1550
1540
1530
1520
P exc = 3 μW
Norm PL
1
0.8
0.6
0.4
0.2
5 K
80 K
0.0
0.1
0.2
1/T (1/K)
Temp:
5 K
CX
80 K
Norm PL intensity (arb. units)
0.800
0.805
0.810
0.815
Energy (eV)

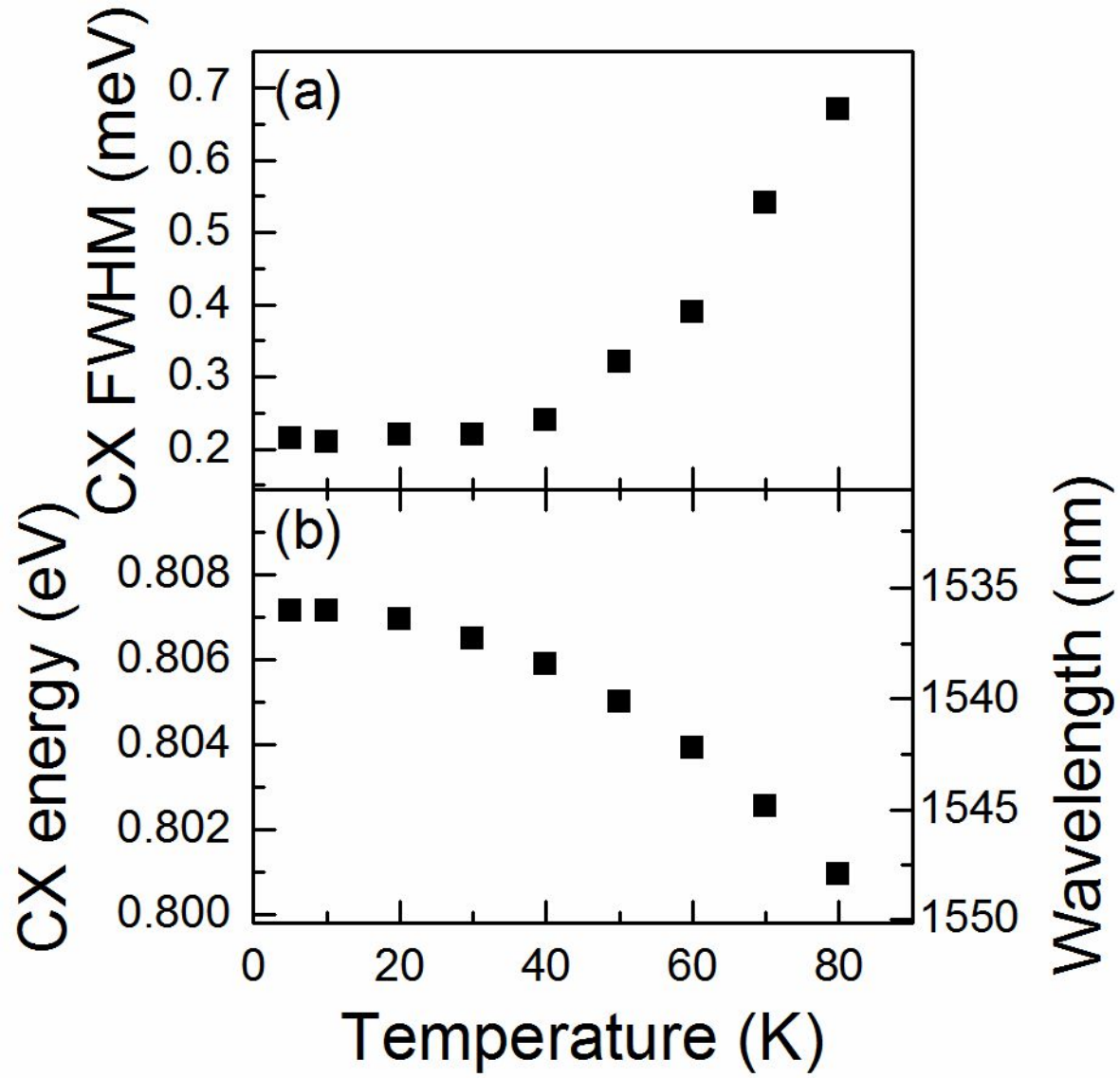
(a)
(b)
CX FWHM (meV)
CX energy (eV)
Wavelength (nm)
Temperature (K)
0.7
0.6
0.5
0.4
0.3
0.2
0.808
0.806
0.804
0.802
0.800
1535
1540
1545
1550
0
20
40
60
80

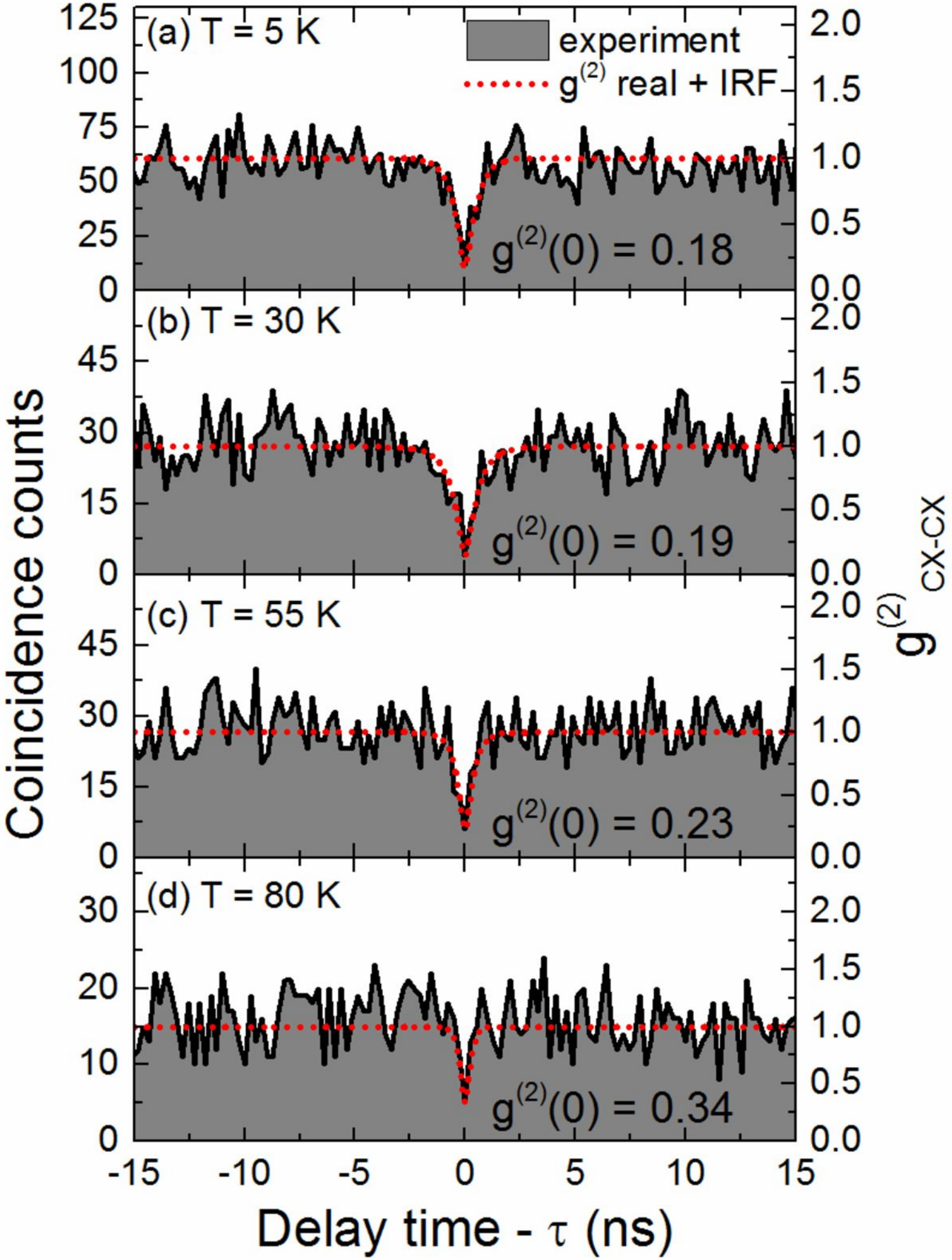
(a) T = 5 K
experiment
g(2) real + IRF
g(2)(0) = 0.18
(b) T = 30 K
g(2)(0) = 0.19
(c) T = 55 K
g(2)(0) = 0.23
(d) T = 80 K
g(2)(0) = 0.34
Coincidence counts
g(2) CX-CX
Delay time - τ (ns)